In The Name of God

Negin Esmaeilzade 97104034

Advanced Neuroscience HW4

Dr. Ali Ghazizade

Part 1.A)

In the first step, we use furrier transform to omit the pink noise. For this purpose, the best linear polynomial is fitted to each LFP signal furrier transform in a logarithmic space to estimate pink noise for each signal. Here is an example for what is done:

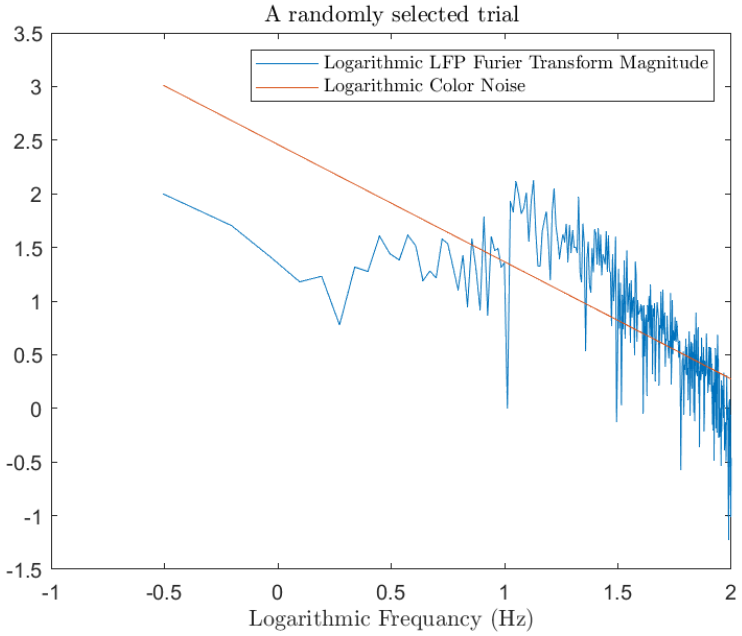

Then the calculated noise is omitted in each signal. After color noise cancelation the average power spectrogram is calculated for each electrode through calculating the power of the furrier transform and taking an average through all trials for each electrode. Below are the resulted average power spectrogram plots for each of the 48 electrodes.

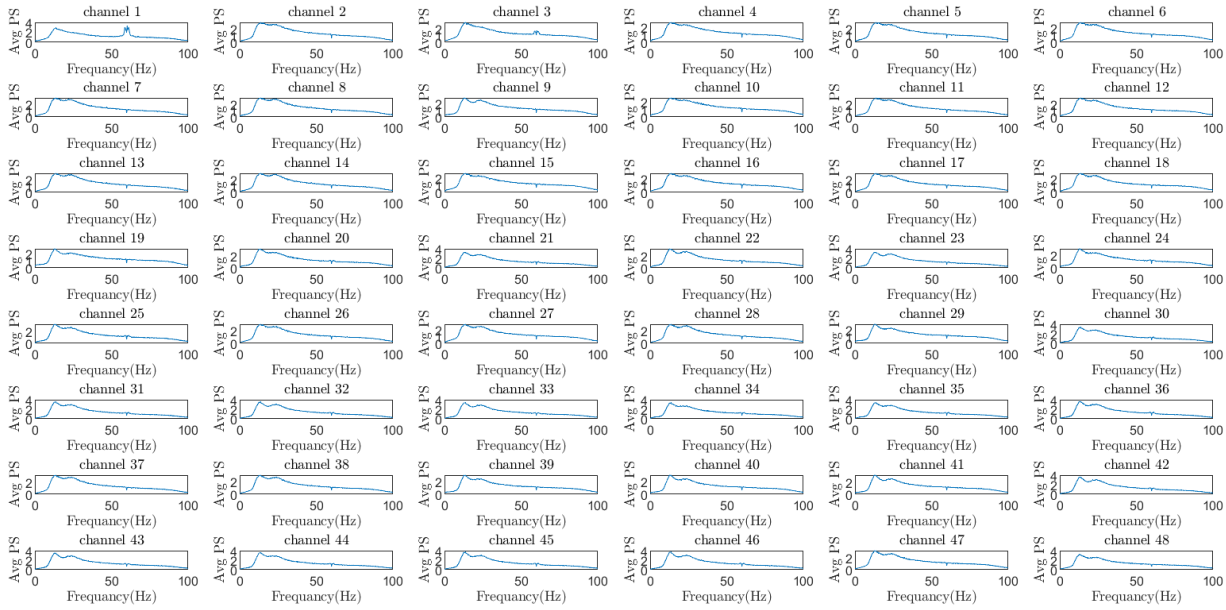

For each electrode the most dominant frequency is calculated through finding the frequency at which leaded to the maximum value for the power spectrum and the figures below show the amounts of these dominant frequencies for each electrode.

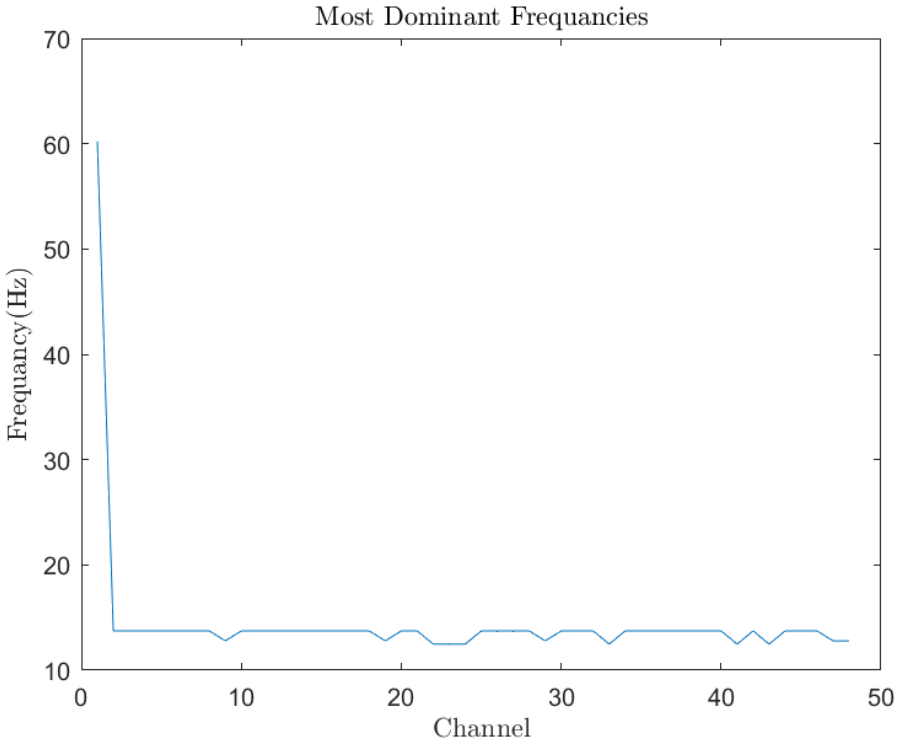

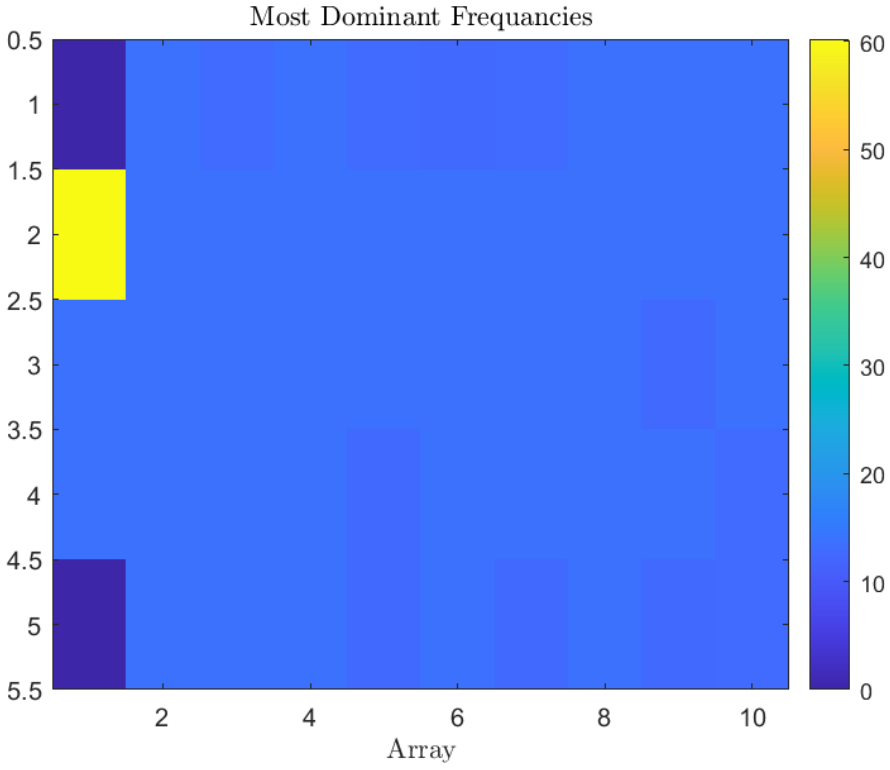

Part 1.B)

In this part, the electrodes are clustered based on their dominant oscillation frequency. As, it could be seen in the previous part, we have overall 4 different dominant frequencies. However, 3 of these are sufficiently close and approximately about 13 Hz. One of this electrode's dominant frequency is too far from the others and about 60 Hz. If we look at the power spectrogram plot of this channel represented in the previous part, we can see that even this channel has a dominant frequency about 13 Hz, but a noisy element caused the maximum power to occur at a different frequency. In fact, we can say that we have only 2 clusters, and regardless to the noisy channel we can say there is only one cluster, and the dominant frequencies are too close. This was expected due to the interconnections between near units and their correlations due to the very close distance, because the array dimension is too smaller in comparison to the cortex. Below is the result of clustering the electrodes dominant frequencies. The exact center of each cluster is shown in the figure.

Notice: we expect that in a microscopic view, we also should see the effect of distance on the topography. Thus, we should see some local clusters in a deeper look. The figure on the next page almost confirms this idea increasing the number of clusters and looking more detailed. However, it is not needed here cause for our analysis the clusters enough close to say that they are almost the same.

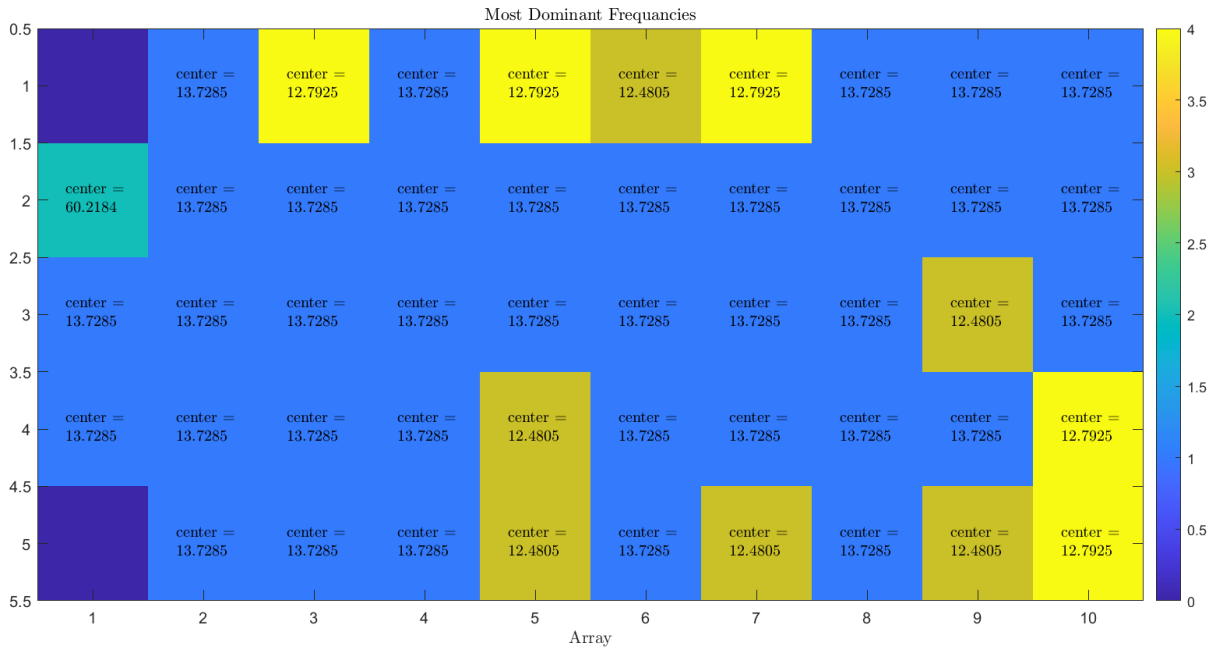

Part 1.C)

In this part, the power spectrum of LFP signals is calculated through the time using the short-time furrier transform. Here is the resulted plot for a randomly selected channel (note that the dominant frequency is reported in the figure):

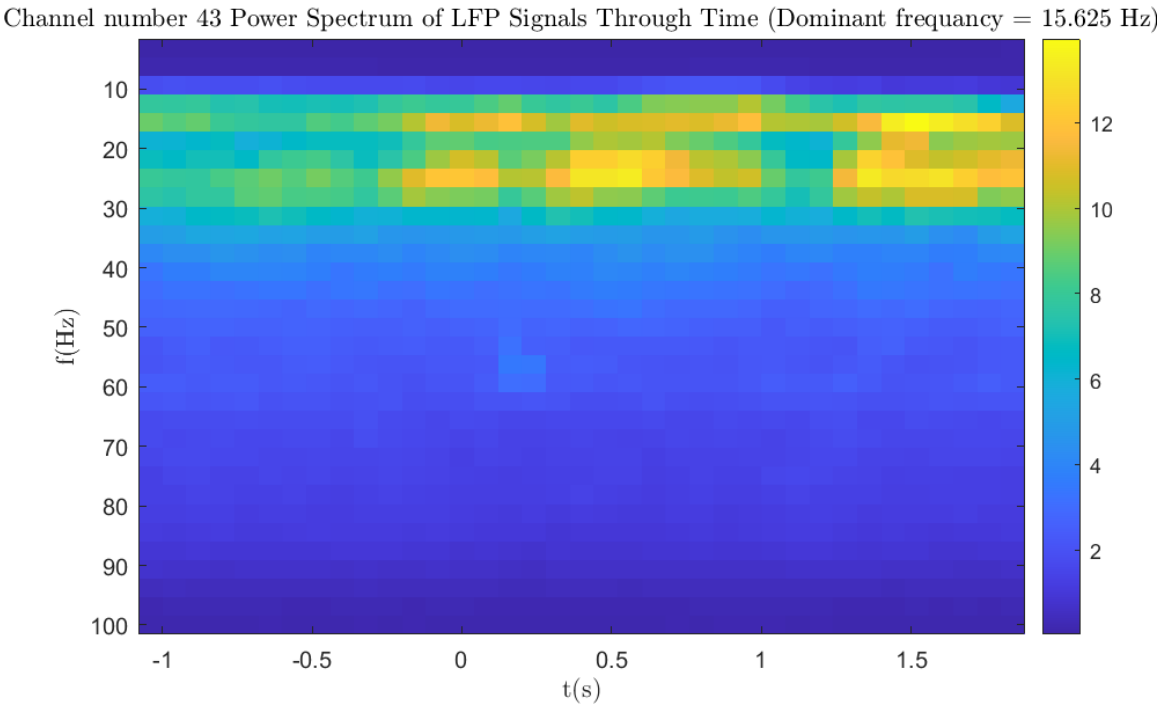

Below is the resulted plot, when taking an average across channels:

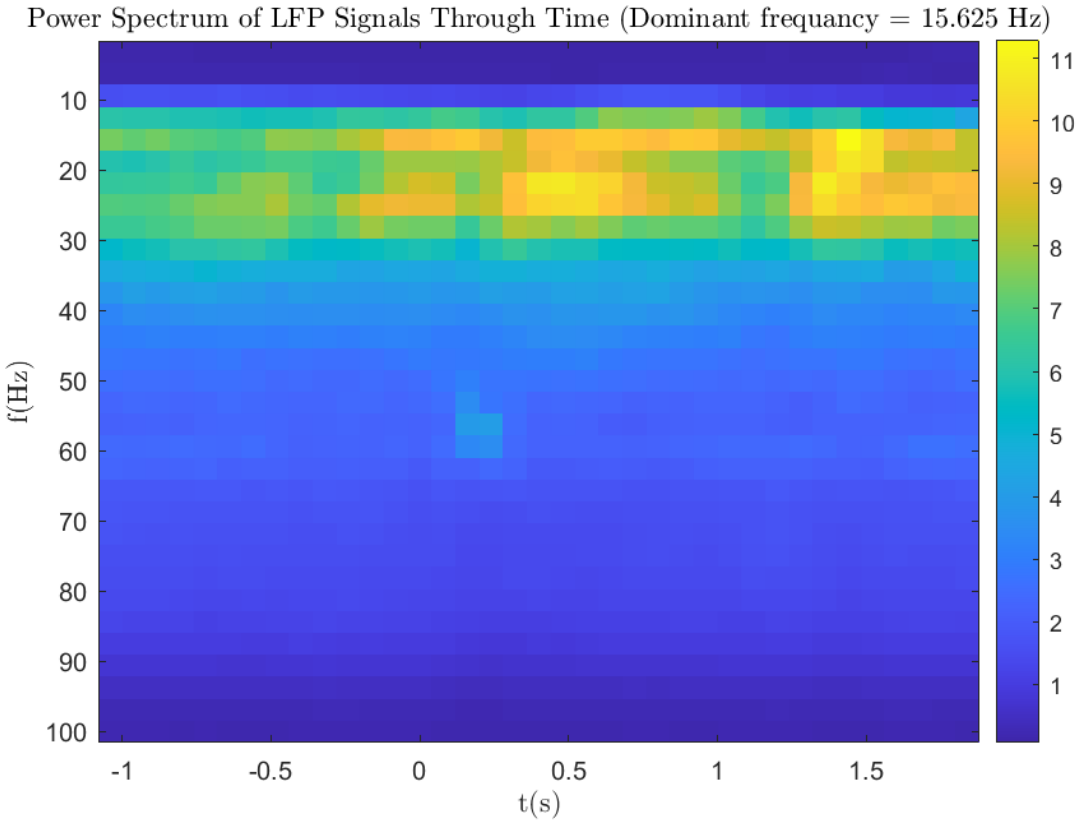

Part 1.D)

As we saw in the previous part the low boundary of beta [8-13] Hz and high boundary of beta [13-30] Hz seem to have more spectral power, in comparison to delta [1-4] Hz and theta [4-8] Hz or gamma low/high [30-150] Hz boundaries. Also, it can be seen in the previous figure that after a short time passes from the stimuli onset, the spectral power increases significantly. In the paper it is shown that the activity of the units is increased within the intervals near to the stimuli onset and it is cited that the major activities were in the higher beta boundaries thus our figure and our results are somewhat similar to the paper's.

Part 2.A)

In this part, a band-pass 2nd order Butterworth filter is used to select the most dominant oscillation of each electrode's LFP signal, considering the central frequency of the filter equal to the electrodes' dominant frequency's cluster's center (13.4696Hz) and 1H bandwidth.

Part 2.B)

Using Hilbert transform and the equation below, the instantaneous phase of filtered signals is calculated and stored in a (5*10*number-of-trails*number-of-time-points) matrix named $\phi(x,y,t)$.

$$s(t) + iHb[s(t)] = a(x,y,t)\, e^{i\phi(x,y,t)}$$

$$\phi(x,y,t) = angle(s(t) + iHb[s(t)])$$

Part 2.C)

$Cos(\phi(x,y,t)$ is measured and the demo is designed during different time points of a randomly selected trial. We can see traveling waves specially after the stimuli onset moving approximately from the right side of the screen to the left.

Part 2.D)

The Phase Gradient Directionality, Direction of Propagation, and Speed of these traveling waves are calculated using these formulas:

$$PGD(t) = \frac{\left|\left|\overline{\nabla\phi}\right|\right|}{||\nabla\phi||},\ Speed(t) = \frac{\left|\overline{\frac{\partial\phi}{\partial t}}\right|}{||\nabla\phi||},\ direction(t) = -\overline{\nabla\phi}$$

Considering electrode distances = 0.4mm as a scaling parameter for ϕ.

Part 2.E)

The calculated traveling waves properties are added to the Demo and the demo is put in the zip file.

Part 2.F)

From the demo we can claim that there is surely a preferred direction propagation for traveling waves cause as it can be seen, it is at least visible that the waves are mostly likely to move from right to left. However, to validate that we can take a look at the direction histogram (considering all trials and for all time samples):

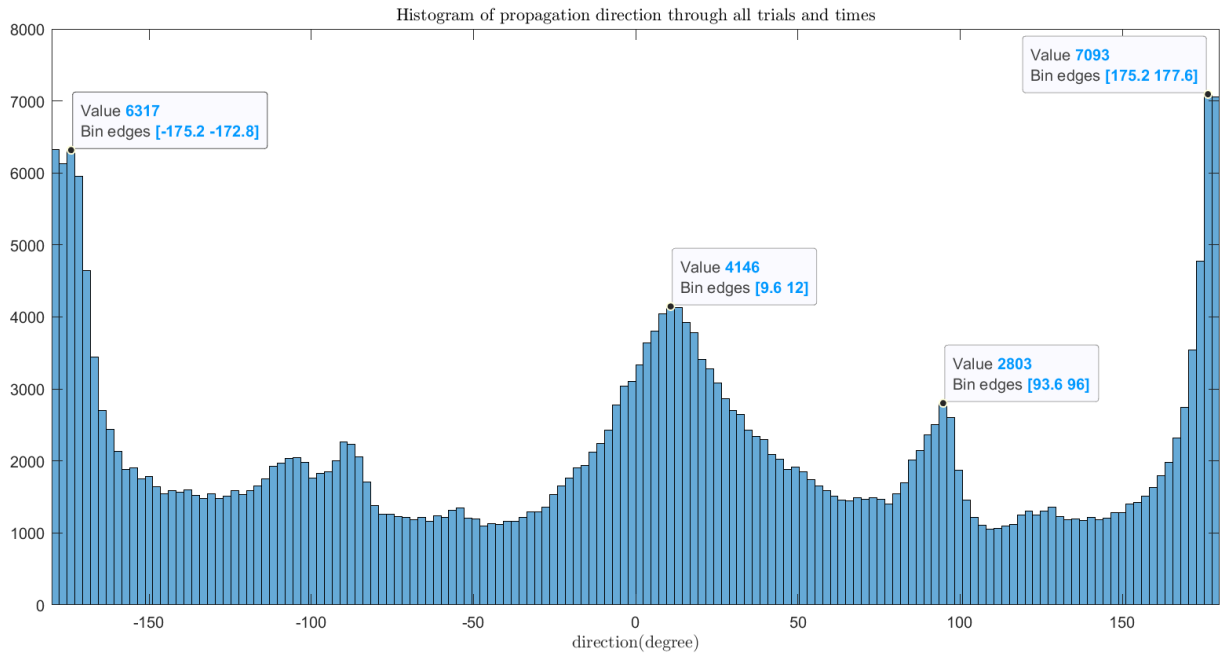

As we can see there are some meaningful peaks in the histogram. Due to the symmetry, we can just notice to the [0,180] degrees interval. We can see that there are two preferred directions of 10.8 degree and 176.4 degree. Another peak can be seen at about the 90 degree which is not important, because it is caused by the topmost and downmost electrodes of the array at which the gradient is forced to be about 90 during a traveling wave exists.

Part 2.G)

Figures below show our results for the histogram of PGD, speed and direction of propagation among all trials. In the paper, they've implied that traveling waves are visible in ECoG, for LFP with multi-electrode-arrays (MEA) with speed of [1-10]m/s for macroscopic, and [10-80]cm/s for mesoscopic waves, in our observations the average speed of propagation is 9.4186 cm/s. As we can see in the histogram the range speeds are almost within the criteria. Note that We've used Hilbert-based phase extraction and this phase-based wave analysis almost discriminates stationary bump form waves.

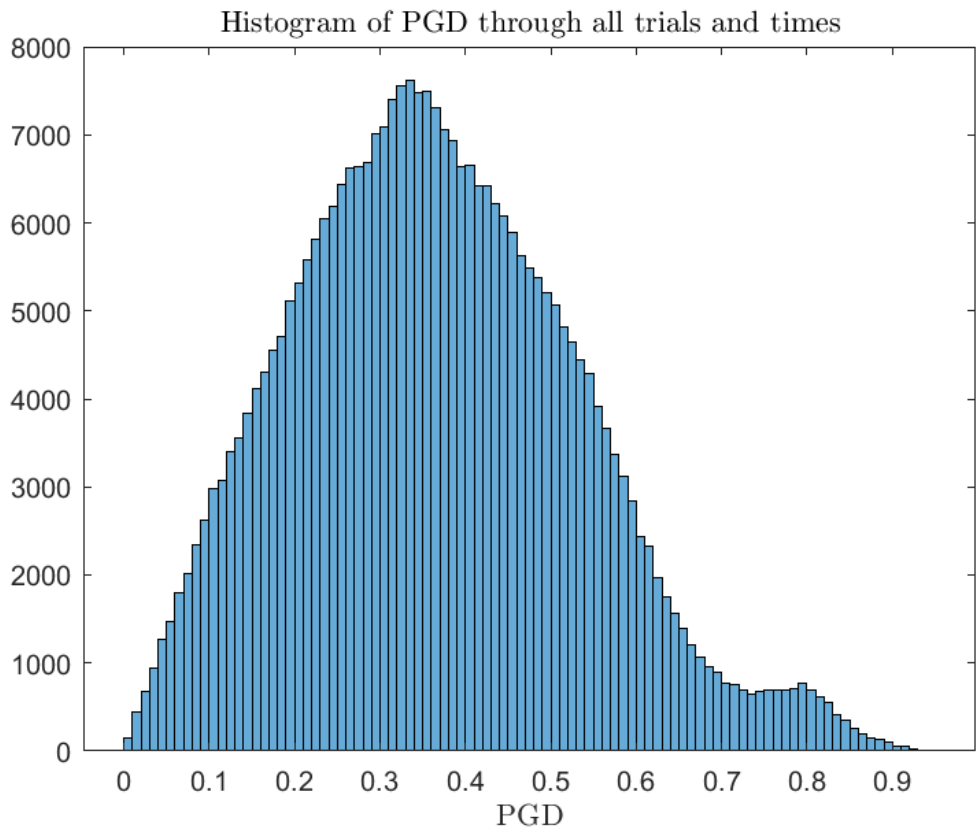
Histogram of PGD through all trials and times
8000
7000
6000
5000
4000
3000
2000
1000
0
0
0.1
0.2
0.3
0.4
0.5
0.6
0.7
0.8
0.9
PGD

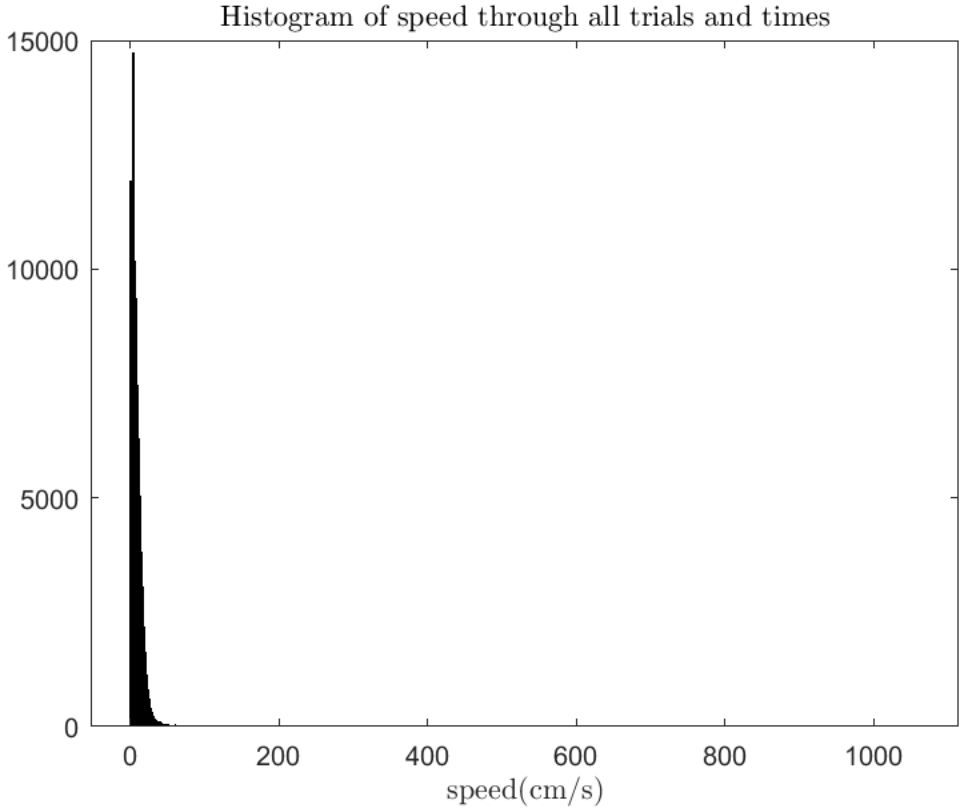
Histogram of speed through all trials and times
15000
10000
5000
0
0
200
400
600
800
1000
speed(cm/s)

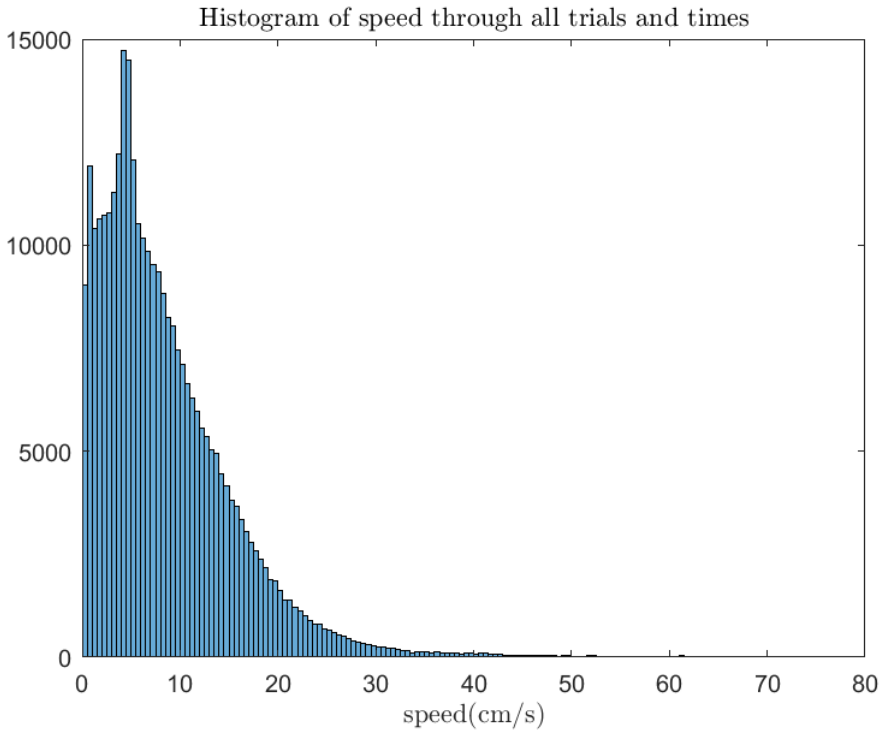
Histogram of speed through all trials and times
15000
10000
5000
0
0
10
20
30
40
50
60
70
80
speed(cm/s)

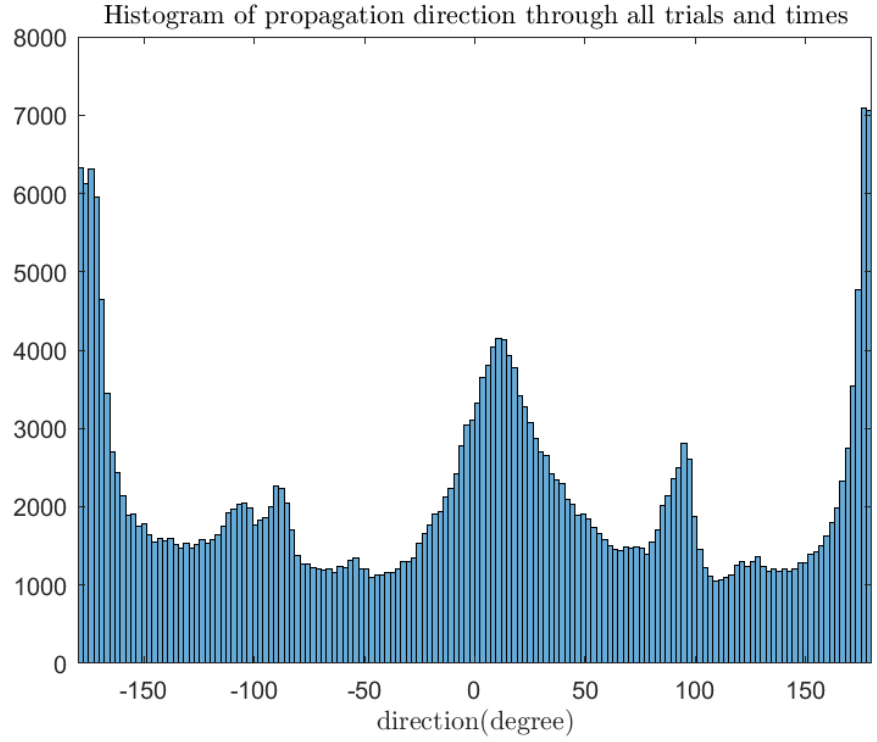
Histogram of propagation direction through all trials and times
8000
7000
6000
5000
4000
3000
2000
1000
0
-150
-100
-50
0
50
100
150
direction(degree)